Dalton Transactions

Accepted Manuscript

ROYAL SOCIETY OF CHEMISTRY

www.rsc.org/dalton

Cite this: DOI: 10.1039/c0xx00000x

www.rsc.org/xxxxxx

ARTICLE TYPE

Conformationally stressed novel ball-type perylenediimide appended zinc(II)phthalocyanine hybrid: spectroelectrochemical, electrocolorimetric and photovoltaic properties

Fatih Pekdemir,[a] Sertan Kurnalı,[b] Abdurrahman Şengül,*[a] Ahmet Altındal,[c] Ali Rıza Özkaya,[d] Bekir Salih[e] and Özer Bekaroğlu*[f]

Received (in XXX, XXX) Xth XXXXXXXXX 20XX, Accepted Xth XXXXXXXXX 20XX
DOI: 10.1039/b000000x

A supramolecule, **6** based on an electron-donor zinc phthalocyanine (ZnPc) and an electron-acceptor perylene diimide (PDI) has been synthesized, and characterized by elemental analysis, UV/Vis, IR, ^{1}H NMR and solid state ^{13}C CPMAS NMR and also MALDI-TOF and ICP mass spectrometry. The PDI appended ZnPc core brings about a geometrical constraint in the molecule with intriguing spectroscopic, electrochemical and photovoltaic properties. The first reduction process of **6** occurs on the PDI core while the first oxidation takes place on the Pc ring. These processes reflect a considerably small HOMO-LUMO gap of 1.50 eV, which has vital importance for optoelectronic applications. In addition, the PDI-based first and second reduction processes of **6** are accompanied by an electrochromic behaviour with the colour changes from dark purple to blue and blue to turquoise, respectively. A Photovoltaic cell involving **6** as the donor and [6,6]-phenyl C_{61} butyric acid methyl ester as the acceptor has been fabricated. The measurements on the effect of annealing temperature on its performance indicated that the annealing process gives rise to a significant increase in the open circuit voltage, the fill factor and the photoconversion efficiency.

1. Introduction

A great deal of work in the fields of solar photochemistry and solar energy conversion is based on nature-inspired porphyrin-quinone arrays as a leading paradigm in designing electron donors and electron acceptors ensembles.[1-4] Among the donors, phthalocyanines (Pcs) which are porphyrin analogues, have been extensively used due to their outstanding optoelectronic properties and structural flexibility required for the practical organic solar cells.[5] Thus, their extended π-conjugated structure provides them with strong absorption in the visible region and redox features that make them as a promising molecular component for artificial photosynthetic apparatus. In the past few years, we have directed our attention to the construction of ball-type Pcs which are a new class of Pcs with additional π-extended conjugation,[6-9] in addition to their different and interesting electrical, electrochemical, electrocatalytic, gas sensing and optical properties in comparison to their parent monomers, as detected by spectroscopic, electrochemical and *in situ* spectroelectrochemical measurements.[8, 10] On the other hand, perylene diimides (PDI)[11, 12] have also been successfully proven to be among the most significant electron acceptors due to their stability, the intense light absorption, rich redox chemistry, and high charge-carrier mobilities, which can be modulated as a function of the substitution pattern.[13]

More recently, covalent systems based on PDI covalently linked to one or two Pc units have also been reported.[14] Both energy and charge transfer dynamics have been observed in these systems upon photo-excitation of the Pc units. All these series of D-A hybrids, dyads,[15-17] triads[18, 19] or polyads[20] were built up by connecting Pc units to PDI through the imido positions, whereas Pc-bounded to PDI at the bay-positions are very scarce, and they were expected to have a better electronic interaction as Pc units or segments introduced at the bay-positions of the PDI core.[15, 21] efficiency of energy transfer mainly depends on to spectral overlap between the energy donor and the acceptor, orientation factors, and the average distance between the donor and the acceptor, in addition to electronic structure of the bridge.[22]

Photovoltaic devices based on organic semiconductors are of high interest because of their unique advantages over inorganic counterparts, such as light weight, low material and processing costs, and mechanical flexibility, thus making them promising candidates for future energy sources. Pc compounds are a suitable choice as an absorber in organic solar cells because of their strong absorption coefficient over a wide range of the solar irradiation spectrum.

In this work, PDI chromophore was appended to the ZnPc with the aim of synthesizing a novel donor-acceptor conjugate (Fig. 1), covering also the spectral window between 400 and 600 nm, where the ZnPc exhibits almost no absorption.[20] The combination of two separate components within one molecule in that way is expected to produce a compound with the modified HOMO-LUMO gap in comparison with those of the combined

compounds, as a results of the possible intramolecular electronic interactions between the two units, and thus, intriguing spectroscopic and electrochemical properties. Furthermore, the molecular structure of this kind of conjugate may be very favourable in the solar cell systems, through a multiple pathway for electronic communications. For these reasons, electrochemical, *in situ* spectroelectrochemical and electrocolorimetric and photovoltaic measurements of **6** were also performed.

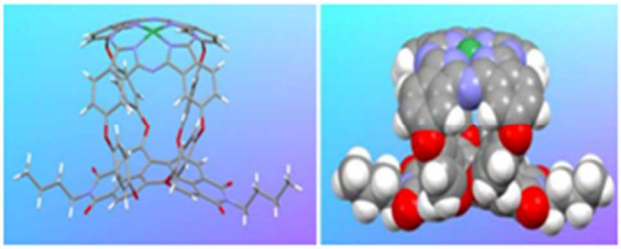

Fig. 1 The optimized structure of **6** calculated at DFT level of theory using B3LYP/6-31G(d) basis set with LanL2DZ on Zn. The ball and stick presentation of the molecule at the left and the space-filling presentation of the molecule at the right side.

2. Results and discussion

2.1. Synthesis

The synthesis of ZnPc-PDI hybrid, **6**, shown in Scheme 1, began with the synthesis and characterization of **2**,[23] **3**[24] and **4**[24] according to previously reported procedures. The compound, 1,6,7,12-tetrachloroperylene tetracarboxylic acid dianhyride **1** is commercially available (ABCR Gmbh & CO.KG) and, was used as received without further purification unless otherwise stated. The tetraphthalonitrile-substituted PDI, **5** was prepared from *N,N*-dibutyl-1,6,7,12-tetrakis(4-hydroxyphenoxy)perylene-3,4:9:10-teracarboxylic acid bisimide (**4**) via nucleophilic displacement of nitro group of 4-nitro-phthalonitrile under inert atmosphere with quite high yield. The cyclic-tetramerization of **5** was accomplished by template reaction in the presence of excess of $Zn(OAc)_2{\cdot}2H_2O$ and a base DBU in dry n-pentanol at reflux under argon to yield very dark purple-black powder with 20% yield (Scheme 1). The compound is thermally stable above 400 °C, and almost insoluble in common organic solvents, but significantly soluble in coordinating solvents such as DMSO, DMF and pyridine, and no significant metal-ligand interactions are expected due to closed-shell d^{10} configuration.[25]

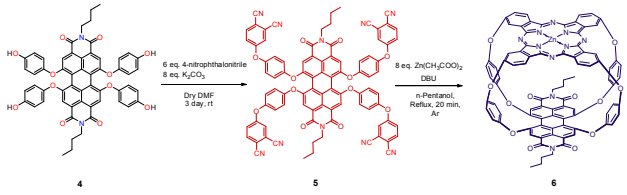

Scheme 1 Synthetic route to **6**.

The first direct evidence for the synthesis of **6** is provided by FT-IR which shows complete disappearance of the cyano stretching at 2232 cm^{-1} observed in the precursor **5**. The experimental and calculated FT-IR spectra are almost identical showing the same pattern of absorption (ESI†, Fig. S8).

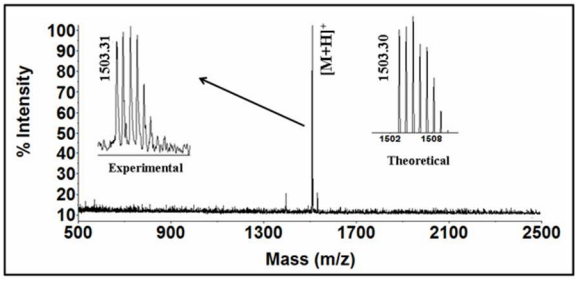

Fig. 2 MALDI-TOF mass spectra of **6**.

High resolution MALDI-TOF mass spectrometry confirmed the expected value of the protonated molecular ion at m/z 1503.31 (calc. m/z 1503.30) as depicted in Fig. 2. It is noticed that the experimental and theoretical isotopic peak distributions are completely matched each other for the complex. No intense fragmentation of the complex was observed. Further proof of this structure being correct is obtained from the ICP mass measurement. For 5.1 mg of **6**, the amount of zinc content was found to be 226 ± 8 ppb (part per billion) experimentally by using ICP-MS. Theoretical value of the zinc content for the 1:1 stoichiometry between organic part and zinc metal in **6** should be 222 ppb. The experimental and the calculated results are in good agreement showing that the experimental value of zinc represented actual structure of **6.** Due to low solubility and also complex structural properties of **6** in which the different aromatic protons had happened to be overlapped , the ^{1}H NMR spectrum is very broad and unresolved (ESI†, Fig. S6). Useful information is still obtained despite the broad peaks as the number of protons in the molecule could be accurately accounted for. In addition, the ratio between the presence of the aliphatic protons on the *N*-butyl groups of the PDI (18H) and the total aromatic protons characteristic to the PDI core and ZnPc subunit (32H) also clearly confirm the structure (ESI†, Fig. S6). Further support of the molecular structure of **6** was obtained by the solid state ^{13}C CPMAS NMR spectrum (ESI†, Fig. S7), in order to shed light onto the ball-type structure as being the novel example among the other hybrids (dyads) with planar side by side structure. The spectrum shows resolved carbon resonances from **6** molecule, and correlates well with the structure as depicted (ESI†, Fig. S7), and supports the success of the synthesis pathway. The integrals of the carbon resonances were not quantitatively determined due to the broad and overlapped nature of the peaks, nevertheless, they qualitatively fit with a correct structure.

The optimized structure shows that the planar 1,4- dioxybenzene bridging units which exert steric congestion in the molecule cause quite significant deviation from the planarity of the ZnPc unit. The perylene core deviates markedly from the planarity in which two naphthalene subunits bend away by 42° according to the calculation. The distortions in the planes of the ring system is very much akin to those of co-facial ball-type dinuclear metallo-phthalocyanines.[9, 26] In this respect, conformationally stressed 1,4,8,11,15,18,22,25-octaisopentyl H_2PcPh_8,[27] domed-shaped metal-free Pc in the solid state,[28] and also metal $PcPh_8$ having saddle-like conformation[29, 30] due to steric hindrance have been reported.[31] The loss of planarity and rigidity of the PDI core and ZnPc subunit in **6** brought about lowering of the extinction coefficients relative to those of the reference compounds as revealed by broadening in the absorption bands of PDI core in the

UV/Vis spectrum of **6** (Fig. 3).

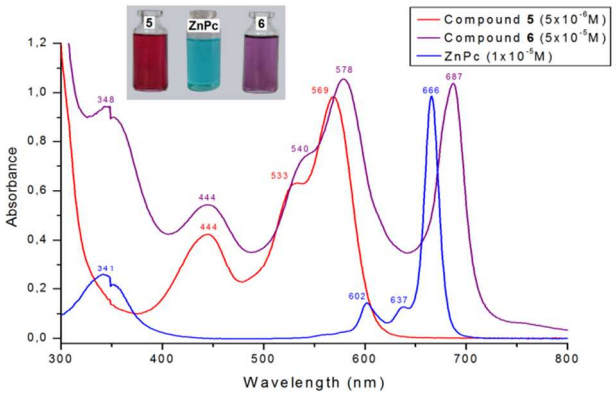

Fig. 3 Absorption spectra of unsubstituted ZnPc (blue), tetra-phthalonitrile-substituted PDI **5** (red) and ZnPc-PDI hybrid **6** (purple) in DMSO recorded at room temperature. The inset shows a photograph of the solutions of **5**, unsubstituted ZnPc and **6** under natural light.

The dihedral angles between the central isoindole units perylene core to result in a dome-shaped Pc ring and twisting of obtained by DFT at the B3LYP/6-31G level provide preliminary insights into the electronic structures and interactions in this D–A hybrid. According to the calculation, the electron distribution of HOMOs was found to be primarily delocalized over the ZnPc, while the electron distribution of the LUMO was found to be predominantly located on the PDI core as depicted in Fig. 4.

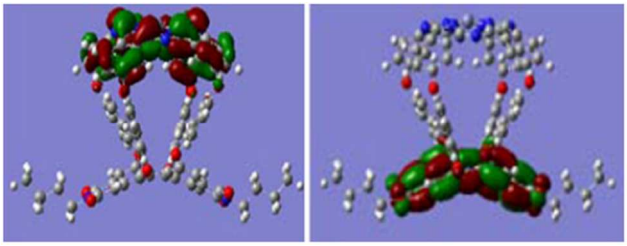

Fig. 4 Schematic representation of the frontier orbitals (left: HOMO, right: LUMO) of the hybrid **6**, computed at B3LYP/6-31G(d) level of theory. The surfaces are generated with isovalue at 0.02.

The calculated absorption spectra of **6** at TD-DFT (B3LYP) using 6-31G(d) basis set are included (ESI†, Fig. S4). As seen in the calculated absorption spectra, experimental tendency is approximately reproduced, although transition energies are slightly overestimated. The absorption bands attributed the perylene core and B-band to the Pc ring are in good agreement with the experimental data. The energy and intensity of the Q-band at TDDFT are underestimated as reported for the related zinc phthalocyanines. [32] The Q-band is related to mainly HOMO → LUMO+1 and less extend to HOMO → LUMO+2 electronic transitions. Discrepancies between the theoretical model and the experiment may due to solvent polarity and the stabilization of the molecule by solvation,[32] in addition to the limitations of the DFT method in describing the excited state.[33, 34] The influence of the degree of nonplanarity on the accuracy of the results obtained from DFT calculations may need to be also carefully accounted for. The energy difference between the HOMO and the LUMO decreases with increasing molecular size,[35] in agreement with the experimental Q-band position (ESI†, Fig. S4). The S1 transition at 760 nm shown as an inset in the figure originates from HOMO → LUMO transition presented in the Table (ESI†, Table S1). This transition is very weak, with oscillator strength of 0.0007, being certainly very difficult to observed experimentally.

The comparison of the UV/Vis spectra of the hybrid **6** with the corresponding precursor **5** and the unsubstituted ZnPc (Fig. 3) show that the macrocyclic components have some electronic interactions in the ground state. The ZnPc reference compound and compound **5** in solution have blue and magenta colour, respectively, while **6** has a very dark purple colour, and absorbs strongly from 300 to 700 nm, making it ideal system to harvest polychromatic light. Moreover, the absorption spectra shown in Fig. 3 are all not expressed as a summation of the spectrum of the constituents, suggesting the presence of interaction between the PDI and ZnPc units in this hybrid.[35] In the UV/Vis spectrum of **6,** a bathochromic shift of the PDI-based absorption band from 569 nm in **5** to 578 nm in **6**, was observed, while the characteristic B- and Q-bands for the phthalocyanines red shifted from 341 nm to 348 nm, and 666 nm to 687 nm, respectively in the unsubstituted ZnPc reference compound and **6**. These changes arise from the substitution at the bay-positions of the PDI core and also may presumably due to an extension of π-conjugation system. The Q-band at 687 nm was considerably red-shifted, less structured and broader compared with those of mono-nuclear ZnPc reference and also of ball-type dinuclear Zn_2Pc_2,[36] in which the corresponding Q-bands observed at 666 and 689 nm,[37] respectively. It is well established that the expansion of π-conjugation in Pcs shifts the Q-band to the red,[38] and also suggest considerable donor-acceptor charge-transfer character in the ground state as in the case of the ethynyl-spaced dyad.[39] In this respect, further support comes from the fluorescence quenching of the PDI chromophore in **6** (ESI†, Fig. S5) as a result of photoinduced charge separation akin to those of DSSCs comprised of ZnPc-PDI dyads.[15, 40]

2.2. Electrochemistry

The redox properties of **6** were studied by cyclic voltammetry, square wave voltammetry, controlled-potential coulometry *in situ* UV/Vis spectroelectrochemistry and *in situ* electrocolorimetry. As shown in Fig. 5A, compound **6** undergoes two well-defined reversible one-electron reductions at the half-peak potentials of $E_{1/2}$ = −0.52 V and $E_{1/2}$ = −0.69 V *vs.* SCE and two weak irreversible one-electron reductions at the cathodic peak potentials of E_{pc} = −1.10 V and E_{pc} = −1.45 V *vs.* SCE. Although it was not possible to monitor any oxidation signal by cyclic voltammetry, square wave voltammetry enabled the recording of the first one-electron oxidation process of **6** at $E_{1/2}$ = +0.98 V *vs.* SCE (upper inset in Fig. 5A). The electrochemical band gap, $E_{elect.g}$ of **6** is 1.50 eV, and much smaller than that of various N,N'-disubstituted PDI compounds (2.1-2.3 eV).[41-46] This low electrochemical band gap is promising for optoelectronic applications. Optical band gap, $E_{opt.g}$ of the complex, calculated additionally from the Pc Q-band absorption at 687 nm in the UV/Vis spectrum, using the Planck equation is 1.80 eV which is higher than $E_{elect.g}$, probably due to the fact that the first reduction process of the complex occurs on the PDI core while the first oxidation process takes place on the Pc ring. The occurrence of the first reduction on the PDI core and the first oxidation on the Pc ring is also compatible with the result of the structure

optimization calculations for **6** as the HOMO is located over the ZnPc subunit and the LUMO is delocalized on the PDI core.

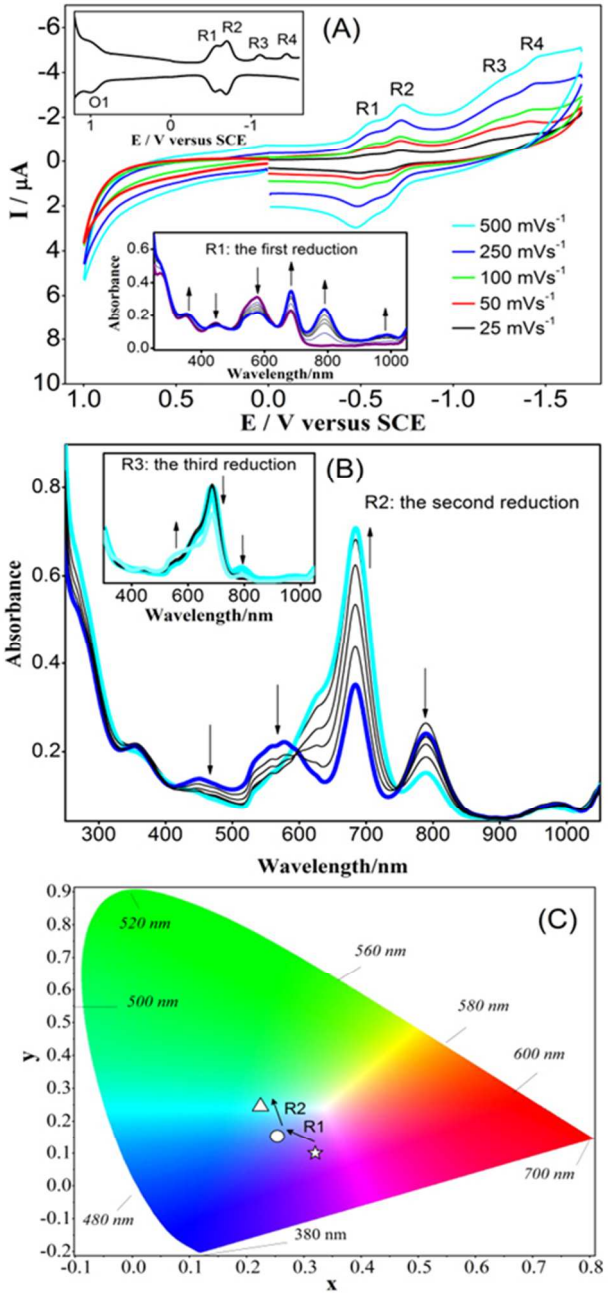

Fig. 5 (A) The cyclic and square wave voltammograms (upper inset) of **6** and in situ UV/Vis spectroelectrochemical changes during its first reduction process in DMSO (lower inset), **(B)** In situ UV/Vis spectroelectrochemical changes during the first reduction process of **6** in DMSO and **(C)** In situ electrochromaticity diagram for the colour changes associated with the first and second reduction processes of **6** in DMSO.

2.3. In situ UV/Vis spectroelectrochemical and electrocolorimetric studies

In situ UV/Vis spectroelectrochemical and electrocolorimetric measurements during the controlled-potential electrolysis of the solution of **6** in DMSO/TBAP electrolyte at suitable peak potentials were also carried out with the aim of identifying the nature of its redox processes, i.e., the processes are PDI-based or Pc-based, and the colour of the redox products. Upon the first reduction of **6** in its dark purple solution in DMSO/TBAP at -0.58 V *vs.* SCE, the absorptions of the broad band at 576 nm and the weak band at 448 nm decreases while that of the peak at 687 nm increase and two new peaks at 789 and 985 nm appear (lower inset in Fig. 5A). These spectral changes are characteristic for the formation of PDI-based radical monoanion[33-35] and accompanied by a colour change from dark purple (x = 0.320 and y = 0.100) to blue (x = 0.254 and y = 0.153) (Fig. 5C). During the second reduction at -0.80 V *vs.* SCE, the band at 789 nm decreases and that at 448 nm disappears whereas the Pc-based one at 687 nm increases (Fig. 5B). At the same time, the band at 576 nm shifts to 628 nm. These changes correspond to the formation PDI-based dianion species[33-35] and associated by the colour change from blue to turquoise (x = 0.224 and y = 0.245). The decrease in the absorption of the band at 687 nm without shift and the formation of a new band between 500-600 nm during the electrolysis at -1.35 V *vs.* SCE suggest that the third reduction process occurs on the Pc-ring (inset in Fig. 5B). The colour change was not observed during the third reduction process. The difference between the third and fourth reduction peaks is 0.35 V, which points out that the last reduction process is also Pc-based.

2.4 Photovoltaic study

The key factors in determining the performance of a solar cell are to measure the current density as a function of the voltage across the cell and determine the performance parameters such as, short circuit current (I_{SC}), open circuit voltage (V_{OC}), fill factor (FF) and photovoltaic conversion efficiency (η) under particular illumination conditions, so called the standard test conditions[36]. The photovoltaic conversion efficiency of a solar cell is defined as,

$$\eta = \frac{V_{oc} \text{x } I_{sc} \text{x FF}}{P_{in}} \quad (1)$$

where FF is given by,

$$FF = \frac{I_{max} x V_{max}}{I_{sc} x V_{oc}} \quad (2)$$

where I_{max} and V_{max} are the current and voltage at the certain point on the I-V characteristics in which the cell delivers the maximum power density. Fig. 6 shows the J–V characteristics of the ITO/PEDOT:PSS/PCBM/ZnPc-PDI/Al devices at various annealing temperatures. The thickness of the organic layers was fixed at around 80 nm. The effect of the annealing temperature on the open circuit voltage of the ITO/PEDOT:PSS/PCBM/ZnPc-PDI/Al cells is shown in Fig. 6. Although the short circuit current of all devices are about 7.5 mA/cm^{-2} irrespective of the annealing temperature, the open circuit voltage of the same cells increases dramatically with the annealing temperature. The short-circuit current density of the unannealed device is 7.40 mA/cm^2, the open-circuit voltage is 0.58 V. With the increase of annealing temperature the device perform better open-circuit voltage, increasing to 1.08 V, while short circuit current remained nearly unchanged, increased to 7.84 mA/cm^2. The origin and limiting factors for the open circuit voltage in organic solar cells is not fully understood. Several recent reports on planar heterojunction as well as bulk heterojunction solar cells have shown that the value of this quantity depends on the energy difference between

the LUMO of the acceptor material and the HOMO of the donor material[37-39]. However, a very recent study on the performances of CuPc/C60 and CuPc/C70 solar cells indicates that the V_{OC} is not governed only by the energy difference between the LUMO of the acceptor and HOMO of the donor material[40]. That means, by considering the previous reports on increasing of V_{OC}, there is some factor, which limits this correlation.

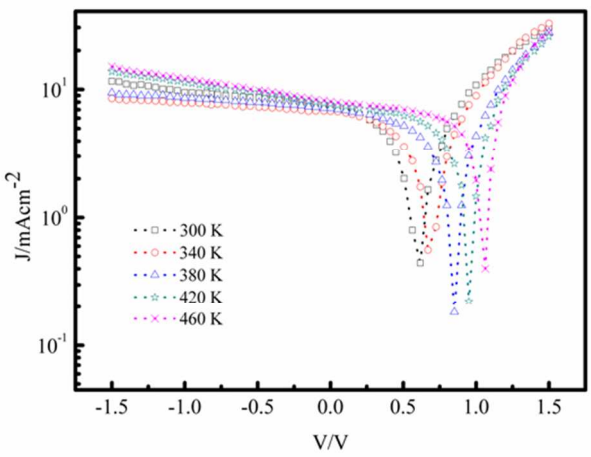

Fig. 6 J-V characteristic of the photovoltaic devices at various annealing temperatures.

In order to investigate the effect of the thermal annealing on performance parameters, we estimated the values of V_{OC}, I_{SC}, FF and η from the analysis of the measured J–V characteristics under illumination. The variations of these parameters with annealing temperature are presented in Fig. 7. As shown in this figure, the V_{OC}, FF and η increases monotonically by increasing annealing temperature. On the other hand, it is also clear that the J_{SC} was not significantly varied with the annealing temperature. Earlier, Pode[40] reported that V_{OC} is significantly dependent on the structure, morphology, strength and width of the absorption spectrum of the film of the donor materials and the efficient separation of charges at the donor/acceptor interface. The effect of the annealing temperature on the observed V_{OC} can be attributed to the increase in the degree of crystallinity, grain size and stacking arrangement of the Pc molecules with increasing annealing temperature. The increase in V_{OC} with annealing temperature reveals that thermal annealing facilitates the separation electrons and holes charge carriers at the donor-acceptor interface in ITO/PEDOT:PSS/PCBM/ZnPc-PDI/Al solar cells. These results also demonstrate explicitly that the V_{OC} is not govern only by the energy difference between the LUMO of the acceptor and HOMO of the donor. As mentioned before, the J_{SC} value was not showed any improvement with annealing temperature. The short-circuit current of a photovoltaic device is generally considered as a combined measure of exciton diffusion towards the donor–acceptor junction and charge transport processes. It is well-known that the heat treatment may cause an increase in the size of domain. As the domain size increases due to the thermal annealing, the interfacial area between donor and acceptor decreases and therefore both the dissociation rate of excitons and the recombination rate decreases, which results in an insignificant improvement of J_{SC}. The fill factor is also strongly dependent upon the loss of charges due to recombination at the maximum power point. The role of domain size is illustrated with the results reported by Jo et al.[41]. They reported that the recombination loss decreases with increasing the domain size. The observed results reveals that the short circuit current and fill factor in ITO/PEDOT:PSS/PCBM/ZnPc-PDI/Al devices are controlled mainly by the increase of grain size with annealing temperature. Power conversion efficiency of the devices varied from 1.72 % to 3.55 % depending upon the annealing temperature. Under AM 1.5G illumination, the device annealed at 420 K showed the maximum η value of 3.55%. The obtained η value is significantly higher than the device fabricated commonly used planar CuPc[42] and non-planar metal Pc[43].

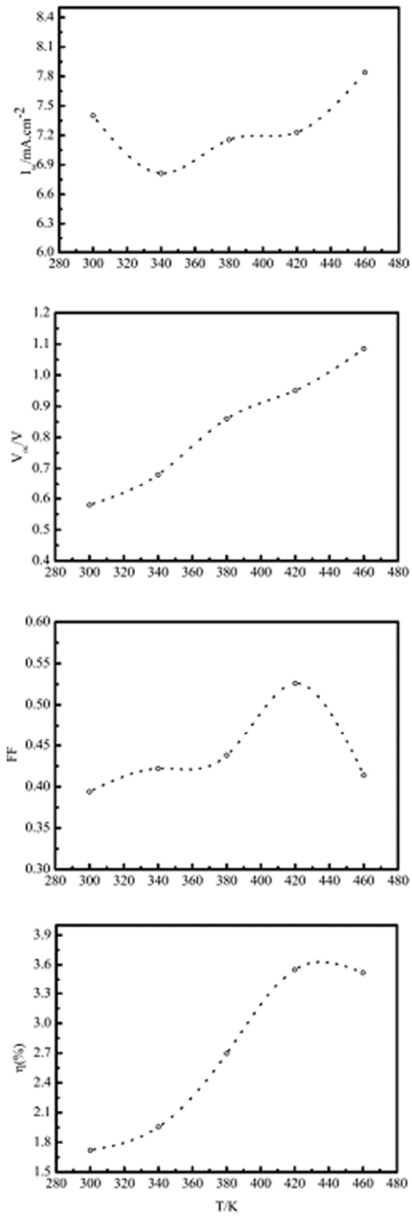

Fig. 7 The dependence of the performance parameters on the annealing temperature.

3. Experimental

3.1. Materials

All chemicals were purchased from commercial sources, and used without further purification. Organic solvents were purified, dried and distilled under dry nitrogen. Compounds **1** and $Zn(OAc)_2{\cdot}2H_2O$ were obtained from commercial suppliers. The starting materials **2**,[23] **3**[24] and **4**[24] were synthesized by the methods as reported previously. These compounds were further purified by column chromatography. The purity of the products was tested in each step by TLC (SiO_2). Chromatography was performed on silica gel 60.

3.2. Equipment

The UV/Vis spectral measurements were carried out with a CARRY 100 Bio UV-Visible spectrophotometer. Fluorescence spectra were measured on a Perkin Elmer LS55 Fluorescence Spectrometer. FT-IR (ATR) spectra with a Perkin Elmer FT-IR Spectra 100 Spectrophotometer at room temperature. Elemental analysis measurements were carried out with a CHNS-932 (LECO) Elemental Analyzer. NMR spectra were measured with a Bruker Ultrashield Plus 400 and with a Varian VNMRS 600 ($CDCl_3$ and DMSO-d_6 as solvent). The solid state ^{13}C CPMAS NMR spectrum was recorded on Bruker 9.4 T NMR spectrometer at ambient temperature, 20 kHz MAS and 600 MHz ^1H Larmor frequency. 2 seconds recycle delay was used for 10 k scans, and 90 kHz proton decoupling was applied during acquisition. 2 ms CP contact time was used. Mass spectra were obtained from a Voyager-DE matrix-assisted laser desorption/ionization time-of-flight (MALDI-TOF) mass spectrometer and with a SCIEX 4000 QTRAP LC-MS/MS mass spectrometer. MALDI matrix, 2,5-dihydroxybenzoic acid was prepared in THF-DMSO (1:1, v/v) containing 0.1% trifluoroacetic acid at a concentration of 10 mg/mL. MALDI sample was prepared by mixing sample solutions (1.0 mg/mL in THF-DMSO-Acetic Acid mixture (1:1:1, v/v/v) having 1% trifluoroacetic acid) with the matrix solution (1:10, v/v) in a 0.5 mL Eppendorf® micro tube. Finally 0.5 µL of this mixture was deposited on the sample plate, dried at room temperature and then analyzed. An inductively coupled plasma mass spectrometer (Thermo FISCHER ICP-MS, Xseries 2, Germany), equipped with a PFA concentric nebulizer (Meinhard Associates, Golden, USA), a quartz cyclonic spray chamber (Glass Expansion, Inc., West Melbourne, Australia), a quartz torch with a quartz injector tube (2 mm i.d.) and an ASX 500 model 520 auto sampler (CETAC, Omaha, NE) was used for zinc measurement. Thermo PlasmaLab 2.6.2.337 version software was used to record data and used to quantify Zn in samples. For ICP-MS analysis, purified complex (5.1 mg) was dissolved in 100 mL 10% acetic acid solution. One mL of this solution was taken and diluted with 10% acetic acid solution up to 10 mL and then analyzed by ICP-MS.

3.3. Synthesis

3.3.1. Synthesis of 5

A solution of **4** (0.2 g, 0.21 mmol, 1.0 eq.) in 30 mL of dry DMF was stirred at rt for 10 min. under argon. To this, 4-nitrophthalonitrile (0.22 g, 1.2 mmol, 6.0 eq.) and K_2CO_3 (0.24g, 1.7 mmol, 8.0 eq.) were added. After stirring the solution at rt for 3 days, and then at 50 ºC for 4 h, the solvent was evaporated under vacuum. The residue was treated with a mixture of 50 mL H_2O in supersonic bath. The product was filtered off and washed with plenty of water. The dark purple product was dried in vacuum (75 ºC). Yield, 83% (0.25 g). M.p.: 328-330 ºC. FT-IR (ATR) (υ): 2957, 2232(C≡N), 1694, 1484, 1277 and 1190 cm^{-1}.
LC-MS (*m/z*): Calcd. for $C_{88}H_{50}N_{10}O_{12}$: 1462.4 $[M+Na]^+$; found: 1463.2 $[M+Na]^+$ (Figure S1). UV-Vis (DMSO) λ_{max} nm (log ε): 444(4.92), 533(5,10), 569(5.29) (Figure S2). ^1H NMR (400MHz, $CDCl_3$): δ 8.21 (s, 4H), 7.73 (m, 4H), 7.22 (m, 8H), 7.02 (m, 16H), 4.08 (t, 4H), 1.60 (m, 4H), 1.36 (m, 4H), 0.89 ppm (t, 6H) (Figure S3).

3.3.2. Synthesis of compound 6

A portion of compound 5 (115.0 mg, 0.08 mmol, 1.0 eq.) and $Zn(OAc)_2{\cdot}2H_2O$ (140.0 mg, 0.64 mmol, 8.0 eq.) in 30 mL of n-pentanol were stirred under argon in a Schlenk tube at rt for 15 minute. Then, DBU (0.25 mL) was added into the mixture. The resulting mixture was refluxed for 20 min. under argon by using the heating gun set to 300 ºC. After cooling to room temperature, the reaction mixture was poured into a 100 mL of hexane, and the precipitate was collected by filtration. The precipitate was boiled with several 100 mL portions of water and collected by filtration. The precipitate was suspended in acetic acid (20 mL) and the insoluble fraction was collected by filtration, and washed with plenty of hot water and methanol, and then dried in vacuum (85 ºC) to yield very dark indigo (wine grapes) colour powder. Yield, 20% (25.0 mg) of **6**. M.p.: > 400 ºC. FT-IR (ATR) (υ cm^{-1}): 2929, 1658, 1588, 1494, 1273 and 1184 (Figure S8). MALDI-TOF-MS (*m/z*): Calcd. for $C_{88}H_{50}N_{10}O_{12}Zn$: 1502.29 $[M]^+$; found: 1503.31 $[M+H]^+$ (Fig. 2). CHN calc. for $C_{88}H_{50}N_{10}O_{12}Zn$: C, 70.23, H, 3.34, N, 9.30; found: C, 70.0, H, 3.6, N, 9.5%. UV-Vis (DMSO) λ_{max} nm (log ε): 348(4,27), 444(4.03), 540(4,16) 578(4.32), 687(4.32) (Figure S4). ^1H NMR (600MHz, DMSO-d_6): δ 8.13 (s, 4H), 7.72-7.01 (m, 28H), 4.35 (t, 4H), 1.66−0.93 ppm (m, 14H) (Figure S6).

3.4. Electrochemistry

Voltammetric measurements were carried out with a Gamry Reference 600 potentiostat/galvanostat combined with a three-electrode configuration at 25 °C. A Pt disc with a surface area of 0.071 cm^2, a Pt wire and a saturated calomel electrode separated from the bulk of the solution by a double bridge (SCE) were employed as the working, counter and reference electrodes, respectively. Electrochemical grade TBAP in extra pure DMSO was employed as the supporting electrolyte at a concentration of 0.10 mol dm^{-3}. *In situ* UV-Vis spectroelectrochemical and *in-situ* electrocolorimetric measurements were carried out under potentiostatic control by an Ocean Optics HR2000+ diode array spectrophotometer, utilizing a three-electrode configuration of a thin-layer quartz spectroelectrochemical cell. The standard illuminant A with 2 degree observer at constant temperature in a light booth designed to exclude external light was used in electrocolorimetric measurements. Prior to each set of measurements, background color coordinates (x, y, and z values) were taken at open-circuit, using the electrolyte solution without the complexes under study. During the measurements, readings were taken as a function of time under kinetic control, however only the color coordinates at the beginning and final of each redox processes were reported.

3.5. Photovoltaic measurements

The photovoltaic device was prepared on patterned indium tin oxide (ITO) coated glass substrates with a sheet resistance of 20 Ω cm^{-2}. The ITO coated substrates were cleaned by ultrasonic

treatment in acetone, isopropyl alcohol, and deionized water. After cleaning, the substrates were dried by N_2 gas. Prior to deposition of the organic layers, the substrates were further treated with UV ozone for 15 min. For the fabrication of the cell, poly(3,4-ethylenedioxythiophene): poly(styrenesulfonate) (PEDOT:PSS) was spin-coated onto the substrates. After thermal annealing of the PEDOT:PSS layer at 120 ºC for 1 h, the active polymer layer, PCBM and Pc was deposited on top of the PEDOT:PSS layer by spin coating method using DMF as solvent. Subsequently, the films were thermally annealed at 150 °C for 15 min to evaporate the solvent. Then, on the top of the organic layer, 500 nm Al layers were evaporated sequentially by thermal evaporation at a pressure below 10^{-5} mbar (Edwards Auto 500). The device current–voltage (I –V) curves were obtained using a Keithley 6517 A electrometer. The measurements of the device characteristics were performed under illumination (100 $mWcm^{-2}$, AM 1.5G) with light provided by a solar simulator.

4. Conclusions

In conclusion, we have designed and successfully synthesized a new type of donor-acceptor conjugate consisting of ZnPc subunit and PDI core bound together through 1,4-dioxybenzene linkages to form geometrically constraint dome-shaped hybrid. Complex **6** displayed four one-electron reduction and a one-electron oxidation processes with an electrochemical band gap of 1.50 eV, which is much smaller than that of previously reported N,N'-disubstituted PDI and promising for optoelectronic applications. *In situ* UV/Vis spectroelectrochemical measurements pointed out that the first and the second reduction processes are PDI-based while the other processes, the first oxidation and the second and the third reductions are Pc-based. Compound **6** displayed well-defined multi-electrochromic behaviour, associated with the perylene-based first and second reduction processes, with colour changes from purple to blue and blue to turquoise, respectively. The effect of the annealing temperature on the photovoltaic performance of ITO/PEDOT:PSS/PCBM/ZnPc-PDI/Al devices have been investigated. Although the short circuit current value has not shown any improvement, the power conversion efficiency, open circuit voltage and fill factor increased with annealing temperature. When all parameters combined, the overall trend is that the optimal annealing temperature for the investigated devices is approximately 425 K.

Acknowledgements

We are grateful to Bülent Ecevit University for the financial support contributed by YÖK-ÖYP programme and Marmara University Scientific Research Commission for their financial support (Project No: FEN-A-150513-0164). Ö.B., B.S. and A.R.Ö. thank Turkish Academy of Sciences, TUBA, for the partial financial support. The authors gratefully acknowledge Dr. Ümit Akbey at the NMR Supported Structural Biology, Leibniz-Institüt für Molekulare Pharmakologie, FMP, Berlin, Germany for the measurement of the solid state CP/MAS ^{13}C NMR.

Notes and references

[a] *Department of Chemistry, Faculty of Arts and Sciences, Bülent Ecevit University, Zonguldak, TR-67100, Turkey.* ***E-mail:*** *fthpekdemir@hotmail.com, sengul@beun.edu.tr;* ***Fax:*** *+90 372 257 41 81 ;* ***Tel:*** *+90 372 257 20 70*

[b] *Department of Physics, Faculty of Arts and Sciences, Bülent Ecevit University, Zonguldak, TR-67100,Turkey.* ***E-mail:*** *sertankurnali@yahoo.com;* ***Fax:*** *+90 372 257 41 81 ;* ***Tel:*** *+90 372 257 20 70*

[c] *Department of Physics, Davutpasa Caddesi, Yıldız Technical University, Esenler, Istanbul, TR-34220, Turkey.* ***E-mail:*** *altindal@yildiz.edu.tr;* ***Fax:*** *+90 212 383 42 34;* ***Tel:*** *+90 212 383 42 31*

[d] *Department of Chemistry, Marmara University, Göztepe, Istanbul, TR-34722, Turkey.* ***E-mail:*** *aliozkaya@marmara.edu.tr;* ***Fax:*** *+90 216 347 87 83;* ***Tel:*** *+90 216 347 96 41*

[e] *Department of Chemistry, Hacettepe University, Beytepe, Ankara, TR-06800, Turkey.* ***E-mail:*** *bekir@hacettepe.edu.tr;* ***Fax:*** *+90 312 288 2163 ;* ***Tel:*** *+90 312 297 7975*

[f] *Department of Chemistry, Istanbul Technical University, Maslak, Istanbul, TR-34469, Turkey.* ***E-mail:*** *obek@itu.edu.tr;* ***Fax:*** *+90 216 3860824 ;****Tel:*** *+90 216 3479641*

† Electronic Supplementary Information (ESI) available: [Synthesis, spectroscopic characterization of the compounds, electrochemical and phtovoltaic measurements and also DFT calculations]. See DOI: 10.1039/b000000x/

1. B. O'Regan and M. Gratzel, *Nature*, 1991, **353**.
2. M. Grätzel, *Inorg. Chem.*, 2005, **44**, 6841-6851.
3. G. J. Meyer, *Inorg. Chem.*, 2005, **44**, 6852-6864.
4. Y. Kobuke, *Eur. J. Inorg. Chem.*, 2006, **2006**, 2333-2351.
5. O. Ito, Y. Araki, S. Uchida, M. Itou, Y. Chen and K. Kitazume, *J. Porphyrins Phthalocyanines*, 2006, **10**, 1190-1196.
6. A. Sengul, H. Z. Dogan, A. Altindal, A. R. Ozkaya, B. Salih and O. Bekaroglu, *Dalton Transactions*, 2012, **41**, 7559-7572.
7. T. Ceyhan, A. Altındal, M. K. Erbil and Ö. Bekaroğlu, *Polyhedron*, 2006, **25**, 737-746.
8. M. S. Agirtas, A. Altindal, B. Salih, S. Saydam and O. Bekaroglu, *Dalton Transactions*, 2011, **40**, 3315-3324.
9. O. Bekaroglu, *Functional Phthalocyanine Molecular Materials*, 2010, **135**, 105-136.
10. A. S. Basak, A. R. Ozkaya, A. Altndal, B. Salih, A. Sengul and O. Bekaroglu, *Dalton Transactions*, 2014, **43**, 5858-5870.
11. C. Li and H. Wonneberger, *Adv. Mater.*, 2012, **24**, 613-636.
12. Y. Ie, T. Uto, N. Yamamoto and Y. Aso, *Chem. Commun.*, 2009, 1213-1215.
13. F. Wurthner, *Chem. Commun.*, 2004, 1564-1579.
14. G. Bottari, G. de la Torre, D. M. Guldi and T. Torres, *Chem. Rev.*, 2010, **110**, 6768-6816.
15. Á. J. Jiménez, F. Spänig, M. S. Rodríguez-Morgade, K. Ohkubo, S. Fukuzumi, D. M. Guldi and T. Torres, *Org. Lett.*, 2007, **9**, 2481-2484.
16. V. M. Blas-Ferrando, J. Ortiz, L. Bouissane, K. Ohkubo, S. Fukuzumi, F. Fernandez-Lazaroa and A. Sastre-Santos, *Chem. Commun.*, 2012, **48**, 6241-6243.
17. S. Fukuzumi, K. Ohkubo, J. Ortiz, A. M. Gutierrez, F. Fernandez-Lazaro and A. Sastre-Santos, *Chemical Communications*, 2005, 3814-3816.
18. M. S. Rodriguez-Morgade, T. Torres, C. Atienza-Castellanos and D. M. Guldi, *J. Am. Chem. Soc.*, 2006, **128**, 15145-15154.
19. Y. Chen, Y. Lin, M. E. El-Khouly, X. D. Zhuang, Y. Araki, O. Ito and W. A. Zhang, *Journal of Physical Chemistry C*, 2007, **111**, 16096-16099.
20. X. Li, L. E. Sinks, B. Rybtchinski and M. R. Wasielewski, *J. Am. Chem. Soc.*, 2004, **126**, 10810-10811.
21. F. Chaignon, M. Falkenstrom, S. Karlsson, E. Blart, F. Odobel and L. Hammarstrom, *Chem. Commun.*, 2007, 64-66.
22. B. Albinsson, M. P. Eng, K. Pettersson and M. U. Winters, *PCCP*, 2007, **9**, 5847-5864.
23. C.-C. You and F. Würthner, *Org. Lett.*, 2004, **6**, 2401-2404.
24. T. E. Kaiser, V. Stepanenko and F. Würthner, *J. Am. Chem. Soc.*, 2009, **131**, 6719-6732.
25. J. Mack and M. J. Stillman, *Inorg. Chem.*, 2001, **40**, 812-814.

26. L. M. Ozer, M. Ozer, A. Altındal, A. R. Ozkaya, B. Salih and O. Bekaroglu, *Dalton Transactions*, 2013.
27. I. Chambrier, M. J. Cook and P. T. Wood, *Chem. Commun.*, 2000, 2133-2134.
28. H.-J. Lee, W. W. Brennessel, J. A. Lessing, W. W. Brucker, J. V. G. Young and S. M. Gorun, *Chem. Commun.*, 2003, 1576-1577.
29. T. Fukuda, S. Homma and N. Kobayashi, *Chem. Commun.*, 2003, 1574-1575.
30. T. Fukuda, K. Ono, S. Homma and N. Kobayashi, *Chem. Lett.*, 2003, **32**, 736-737.
31. T. Fukuda, S. Homma and N. Kobayashi, *Chemistry – A European Journal*, 2005, **11**, 5205-5216.
32. L. T. Ueno, C. C. Jayme, L. R. Silva, E. B. Pereira, S. M. d. Oliveira and A. E. H. Machado, *Journal of the Brazilian Chemical Society*, 2012, **23**, 2237-2247.
33. E. Gutiérrez-Meza, R. Noria, G. Granados, V. Gómez-Vidales, J. Z. Ramírez, H. I. Beltrán and J. Peon, *The Journal of Physical Chemistry B*, 2012, **116**, 14107-14114.
34. L. Q. Guo, D. E. Ellis, B. M. Hoffman and Y. Ishikawa, *Inorg. Chem.*, 1996, **35**, 5304-5312.
35. N. Shibata, S. Mori, M. Hayashi, M. Umeda, E. Tokunaga, M. Shiro, H. Sato, T. Hoshi and N. Kobayashi, *Chem. Commun.*, 2014, **50**, 3040-3043.
36. S. Altun, A. Altındal, A. Rıza Özkaya, M. Bulut and Ö. Bekaroğlu, *Tetrahedron Lett.*, 2008, **49**, 4483-4486.
37. A. S. Basak, A. R. Ozkaya, A. Altndal, B. Salih, A. Sengul and O. Bekaroglu, *Dalton Transactions*, 2014.
38. S. G. Makarov, O. N. Suvorova, C. Litwinski, E. A. Ermilov, B. Röder, O. Tsaryova, T. Dülcks and D. Wöhrle, *Eur. J. Inorg. Chem.*, 2007, **2007**, 546-552.
39. A. Gonzalez-Cabello, P. Vazquez, T. Torres and D. M. Guldi, *J. Org. Chem.*, 2003, **68**, 8635-8642.
40. D. K. Panda, F. S. Goodson, S. Ray and S. Saha, *Chem. Commun.*, 2014, **50**, 5358-5360.
41. S. K. Lee, Y. B. Zu, A. Herrmann, Y. Geerts, K. Mullen and A. J. Bard, *J. Am. Chem. Soc.*, 1999, **121**, 3513-3520.
42. S. Asir, A. S. Demir and H. Icil, *Dyes and Pigments*, 2010, **84**, 1-13.
43. S. Chen, Y. Liu, W. Qiu, X. Sun, Y. Ma and D. Zhu, *Chem. Mater.*, 2005, **17**, 2208-2215.
44. B. J. Slater, E. S. Davies, S. P. Argent, H. Nowell, W. Lewis, A. J. Blake and N. R. Champness, *Chemistry – A European Journal*, 2011, **17**, 14746-14751.
45. L. Perrin and P. Hudhomme, *Eur. J. Org. Chem.*, 2011, **2011**, 5427-5440.
46. B. A. Llewellyn, A. G. Slater, G. Goretzki, T. L. Easun, X. Z. Sun, E. S. Davies, S. P. Argent, W. Lewis, A. Beeby, M. W. George and N. R. Champness, *Dalton Transactions*, 2014, **43**, 85-94.

Conformationally stressed novel ball-type Zinc(II)phthalocyanine-perylenediimide conjugate: spectroelectrochemical, electrocolorimetric and photovoltaic properties

Fatih Pekdemir, Sertan Kurnalı, Abdurrahman Şengül, Ahmet Altındal, Ali Rıza Özkaya, Bekir Salih and Özer Bekaroğlu

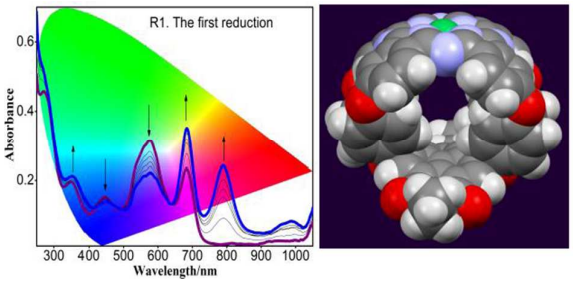

The ZnPc-perylenediimide hybrid displayed well-defined electrochromic behaviour and the best photovoltaic conversion efficiency observed with a Pc-based organic solar cell.